Intermetallics. Vol. 16. Núm. 9. 2008. Pag. 1073-1082
http://dx.doi.org/10.1016/j.intermet.2008.06.006

Mechanical alloying of $Fe_{100-x-y}Nb_xB_y$ (x=5, 10; y=10, 15): From pure powder mixture to amorphous phase

J.J. Ipus, J.S. Blázquez, V. Franco, A. Conde*

Dpto. Física de la Materia Condensada, ICMSE-CSIC, Universidad de Sevilla, P.O. Box 1065, 41080, Sevilla, Spain.

Abstract

The mechanical alloying process of $Fe_{75}Nb_{10}B_{15}$ and $Fe_{85}Nb_5B_{10}$ systems has been studied from an initial mixture of elemental powders. The amorphization process is monitored by X-ray diffraction, Mössbauer spectroscopy and magnetization measurements. An amorphous phase (with a Curie temperature of ~250 K) is formed after 400 h milling only for $Fe_{75}Nb_{10}B_{15}$ alloy, whereas a bcc supersatured solid solution is the final product after milling $Fe_{85}Nb_5B_{10}$ alloy. For both cases, a dispersion of ~10 % in the Fe content of the powder particles persists after 400 h milling. Powder particle size, Cr content and lattice parameter of bcc phase are larger for the alloy with the highest Nb content.

Keywords: A. Nanostructured intermetallics; A. Magnetic intermetallics; C. Mechanical alloying and milling.

*Corresponding author: Prof. A. Conde

Departamento de Física de la Materia Condensada. Universidad de Sevilla.

Apartado 1065, 41080 Sevilla (Spain).

Phone : (34) 95 455 28 85/ Fax : (34) 95 461 20 97

E-mail: conde@us.es

Intermetallics. Vol. 16. Núm. 9. 2008. Pag. 1073-1082
http://dx.doi.org/10.1016/j.intermet.2008.06.006

1 Introduction

Nanocrystalline materials are defined by a crystal size below 100 nm. As a limit, amorphous materials are solid systems where the structural long range order is lost. These materials have received much attention due to their physical properties (mechanical and magnetic), which are clearly different from those exhibited by conventional microstructures and, in some cases, improve their technological applicability [1,2,3]. One way to obtain nanocrystalline materials is by partial devitrification of a precursor amorphous alloy during controlled thermal annealing. This technique controls the microstructure of materials and thus optimizes the properties of the final product. Another possibility is mechanical alloying, which has become a very versatile technique to directly produce metastable microstructures (amorphous, nanocrystallines, supersaturate solid solution, etc) [1] from elemental powders or alloys. During this milling process the material is submitted to fracture and cold welding phenomena, as well as intensive plastic deformation, which define the powder morphology, microstruture and properties. The continuous storing of defects in the crystalline phase during milling process unstabilizes it, leading to nanocrystalline and/or amorphous structures [1].

Nanocrystalline Fe-M-B type alloys (M= Zr, Nb, etc), so-called Nanoperm [4], are attractive due to their soft magnetic properties after optimum thermal treatment and are used in commercial applications such as telecommunications, micro devices and power electronics [5,6]. Although these systems are generally obtained by rapid quenching and subsequent annealing, nanocrystalline alloys of these compositions can be directly obtained by mechanical alloying of elemental powders. As soft magnetic properties depend on the structure of the material [7,8,9], its structural characterization

is a very important task to understand the system behavior and to predict its possible technological capabilities.

In this study, two $Fe_{100-x-y}Nb_xB_y$ (x=5, y=10 and x=10, y=15) alloys were produced by mechanical alloying from a mixture of pure elements and their morphological, compositional and microstructural evolution, as well as their thermal stability, were studied as a function of milling time. The amorphization of the ternary FeNbB system by rapid quenching methods has been studied previously [10]. Whereas compositions similar to Nb10 can be obtained in amorphous structure, those similar to Nb5 can not be obtained as amorphous.

2 Experimental

$Fe_{100-x-y}Nb_xB_y$ (x=5, y=10 and x=10, y=15) compositions were prepared by ball milling in a planetary mill Fritsch Pulverisette 4 Vario from elemental powders (≥ 99 % purity), with particle size d <200 μm for Fe and Nb and d <1 mm for B. For simplicity, the studied alloys will be named in the following by their Nb content: Nb10 for $Fe_{75}Nb_{10}B_{15}$ and Nb5 for $Fe_{85}Nb_5B_{10}$. The initial powder mass was 30 g and the ball to powder ratio was 10:1. The rotational speed of the disk which supports the vials was 150 rpm and that of the vials was 300 rpm in opposite direction. After selected times, some powder was taken out from the vials to characterize the morphology, composition, microstructure and thermal evolution. The opening and closing of the vials was done under argon atmosphere in a Saffron Omega glove box to avoid oxygen and humidity contamination.

Particle size distribution and morphology were studied by scanning electron microscopy (SEM) using secondary electrons (SE) and backscattered electrons (BSE) modes in a Jeol JSM-6460 LV operated at 30 kV. Compositional evolution was studied

Intermetallics. Vol. 16. Núm. 9. 2008. Pag. 1073-1082
http://dx.doi.org/10.1016/j.intermet.2008.06.006

by energy dispersive X-ray (EDX) analysis using an Incax-sight of Oxford Instruments. Phase composition and structure were studied from X-ray diffraction (XRD), using Cu Kα radiation, and Mössbauer spectrometry (MS). Mössbauer spectra were recorded at room temperature in a transmission geometry using a ^{57}Co(Rh) source. Values of the hyperfine parameters were obtained by fitting with NORMOS program [11]. The isomer shift, *I*, was quoted relative to that of α-Fe at room temperature.

Magnetization was measured using a maximum applied field of 1.5 T, in the temperature range from 77 to 440 K, every 15 K, in a vibrating sample magnetometer (VSM). The values of magnetization were obtained by extrapolation to zero field of the linear fitting of the high field magnetization. Thermal characterization of the samples was studied by differential scanning calorimetry (DSC) using a Perkin-Elmer DSC7 in Ar atmosphere.

3 Results

3.1 Morphology and composition

Figure 1 shows SEM images of both alloys obtained after different milling times. For both alloys at short milling times, t <20 h, the particles are formed by joint layers and inclusions, which present different composition. In order to appreciate this heterogeneity in more detail, figure 2 shows SE (figure 2a) and BSE (figure 2b) images taken on a typical particle after 2 h milling for Nb10 alloy. Figure 2c shows EDX spectra taken on the different points marked in figure 2a. The A spectrum, on a dark inclusion, only shows the emission line of boron besides the typical background at low energy, so this zone is rich in this light element. The B and C spectra show zones rich in Fe and Nb, respectively. Therefore, the heterogeneity of the individual powder particles is evidenced for short milling times in the conditions used in this study.

After 20 h milling, the powders show pores and cracks on their surface for Nb10 and Nb5 alloys but no clear layers and, for longer milling times, t ≥100 h, agglomeration of powder is observed. This process seems to depend on milling conditions, as other author have detected agglomeration of particles much earlier for similar compositions (e.g. after 5 and 15 h for $Fe_{84}Nb_7B_9$ alloy with more energetic milling conditions [12]). The particles that form these agglomerates are larger for Nb10 than for Nb5 alloy. After 400 h milling, the agglomerates are not observed for Nb10 alloy but, for Nb5 alloy, the particles are still agglomerated.

From SEM images, a statistical analysis of the average particle size evolution, $<d>$, has been performed over ~100 particles per sample (Figure 3) for both alloys. After 20 h milling, $<d>$ increases over $<d> > 200$ μm for both alloys. As milling time increases, a decrease in $<d>$ is observed and, about 100 h milling, this value is stabilized, being smaller for Nb5 alloy (~ 25 μm) than for Nb10 alloy (~ 50 μm). This indicates that a stationary situation between cold welding and fracture has been achieved.

The compositional evolution was studied by EDX from a statistical set of ~20 particles of each sample. As B content cannot be quantitatively measured by EDX, compositional analysis of the systems is referred to the relative amounts of Fe and Nb. In figure 4, histograms of Fe content of the powder particles are presented for Nb10 and Nb5 alloys after different milling times. For short milling times, t ≤5 h, it is possible to find Nb rich particles and a high fraction of Fe rich particles in both alloys. After 10 h milling, in Nb5 alloy a strong reduction in the broadening of the compositional distribution, ΔC_{Fe}, is observed (calculated as the difference in Fe/Fe+Nb ratio between the Fe richest and the Fe poorest powder particles found). However, this reduction occurs for 20 h in the Nb10 alloy, being a wider compositional distribution for the alloy

with a higher Nb content. For longer milling times, t > 20 h, the broadening of the distribution of Fe content is almost constant and, at the end of the studied range, there is not a unique composition but a certain broadening is found (ΔC_{Fe} =16 at. % of Fe for Nb10 and 8 at. % of Fe for Nb5).

Small Fe contamination is hard to measure in such Fe rich compositions. However, Cr is easily quantified as the initial powder mixture of this study is Cr free. Therefore, figure 5 shows the Cr concentration as a function of the milling time. For both alloys, a linear increase with the milling time is observed in the explored range, being the amount of Cr higher for Nb10 (~2 at. %) alloy than for Nb5 (~1 at. %) alloy after 400 h milling, in agreement with the expected increase of hardness as Nb increases in Fe based alloys [13]. Similar Cr contamination has been found in other ball milled systems [14].

3.2 Structural evolution

3.2.1 X-ray diffraction

Figure 6 shows the XRD patterns of both alloys as a function of milling time. For short milling times, $t \leq 20$ h, a slight broadening of (110) diffraction peak of the α-Fe phase can be observed for both alloys. The full width at half maximum (FWHM) is approximately the same for both alloys at this stage; FWHM increases from 0.26 to 0.52 ± 0.10º from 1 to 20 h, respectively. This effect can be related with the decrease of the crystalline size and an increase of microstrains.

After 50 h milling, a strong broadening of (110) peak is observed, as well as a shift to lower values of 2θ position of this peak. Moreover, the different maxima of bcc-Nb are no longer detected. These effects are related to the Nb incorporation into the bcc-Fe lattice and to the formation of the supersaturated solid solution. For longer milling

times, t >200 h, the XRD pattern of Nb10 alloy shows a halo centered at 2θ ~ 44º and the α-Fe (200) peak is reduced, being unappreciable for t =400h. This is related to the formation of the amorphous phase in the powder particles.

3.2.2 Mössbauer spectrometry

Mössbauer spectra along with the hyperfine magnetic field distributions of the different samples are shown in figures 7 and 8 for Nb10 and Nb5, respectively. Mössbauer spectra were fitted using a ferromagnetic site contribution with HF =33 T for pure α-Fe phase (site-F) and two hyperfine magnetic field distributions; one for low field contributions, D1 (from 0 to 10 T) and other for high field contributions, D2 (>8 T). Furthermore, other site contribution but paramagnetic with quadrupolar splitting ~0.5 mm/s (site-P) is necessary to fit the spectra of Nb10 for long milling times. It is worth mentioning that, for such complex systems as the studied here, there is ambiguity between low field ferromagnetic sites (< 5 T) and paramagnetic ones. For t ≤10 h milling, the spectra only show a sextet with narrow absorption peak (width ~0.30 mm/s) and hyperfine magnetic field 33 T for both alloys, indicating that the α-Fe lattice has not been significantly affected by milling, in agreement with EDX (heterogeneous powder particles, not really alloyed) and XRD (lattice parameter close to pure α-Fe) results.

For Nb10 alloy spectra at t ≥ 20 h, two new contributions appear, D1 and D2. This shows the existence of Fe atoms in three different main environments: first (site-F), pure bcc-Fe phase environment; second (D1), Nb rich environments; and third (D2), Fe rich environments. This latter contribution can be related with Fe atoms in the α-Fe phase but in the presence of impurities of Nb, B and/or Cr (due to contamination by the grinding media) or to Fe atoms at the interface region of nanocrystals [15]. However, in the Nb5 alloy, along with the crystalline contribution, site-F, only the D2 distribution is

observed (D1 is negligible). This means that, in Nb5 alloy, Nb rich environments are not as significant as in Nb10 alloy, as it would be expected.

4 Discussion

4.1 Simulation of powder size evolution

As it was previously mentioned, for 20 h milling, cracks are observed in the particles surface, which may cause the fracture of the particles when the milling continues. The change in the evolution trend of <*d*> could be ascribed to changes in the mechanical properties of the system due to rapid accumulation of defects into the particles [16]. This changes the balance between the two processes responsible for the evolution of <*d*>: fracture and cold welding. In fact, a qualitative change in the mechanical behavior of the powder is clearly observed for milling times longer than 50 h. Until 50 h milling, the powder sticks on the vial wall and ball surface. However, for longer milling times the powder detaches from milling media surfaces, noticeably increasing the amount of loose powder.

Based on these two processes, a basic simulation algorithm was performed to obtain a first approximation of the tendency followed by <*d*> during milling. The initial system consist of 500 equally sized particles. Once a random particle is chosen, its probability to be cold welded with another particle is defined by P_{cw} =exp(-d_i/d_c). This expression depends on the size of the *i* particle, d_i, and a critical size, d_c. Particles with $d_i > d_c$ will tend to fracture, while if $d_i < d_c$, the particle will tend to join with another. As can be inferred from the experimental evolution of <*d*>, d_c is not constant during the milling process. In our simple simulation, only two different values of d_c were used (supported by the abrupt change in the mechanical properties detected between 20 and 50 h. A *dc* value 100 times the initial size was used to reproduce the rapid increase in <*d*> at short milling times. For long milling times, the constant experimental value of

Intermetallics. Vol. 16. Núm. 9. 2008. Pag. 1073-1082
http://dx.doi.org/10.1016/j.intermet.2008.06.006

<*d*> was used as d_c. Simulation results reproduce the experimental ones after properly rescaling the iteration steps with the milling time (see figure 3).

4.2 Simulation of compositional evolution

EDX results indicate that the composition of particles is not unique, even at long milling time but compositional distributions achieve a stationary situation. The parameter ΔC_{Fe} was simulated considered a system of particles defined by a 100 components binary array, being 0 for Nb and 1 for Fe (1 % in compositional resolution). Two random particles will interact changing a portion of their arrays with the same aleatory size. Therefore, powder particles size and number remain unchanged and only compositional evolution is simulated in this very simple simulation. Results are shown in figure 9a along with experimental ones for comparison. Experimental and simulation results agree even quantitatively (once iteration steps are conveniently rescaled), showing a stationary situation of the system with a compositional distribution and, therefore, the existence of a certain degree of heterogeneity (ΔC_{Fe} =18 at. % of Fe for Nb10 and 14 at. % of Fe for Nb5).

Other parameter which enables to follow the compositional evolution is the most probable Fe content in the particles, C_{Fe}, (shown in figure 9b). This parameter rapidly decreases with the milling time close to the nominal composition for both alloys. After 20 h milling, C_{Fe}= 89 and 95 ± 2 at. % for Nb10 and Nb5, respectively. An increase with respect to the nominal compositions (88 and 94 at. % for Nb10 and Nb5, respectively), although into the experimental error, would not be surprising and could be expected due to Fe contamination from milling media. The evolution of C_{Fe} was also obtained from the simple simulation described above (also shown in figure 9b, using the

same iteration step/milling time ratio than for figure 9a) and a good agreement with the experimental data was also found.

4.3 Microstructural evolution

4.3.1 X-ray diffraction

The broadening observed from 20 to 50 h milling in the α-Fe (110) peak is bigger for Nb10 (FWHM =1.55 ± 0.10º) than for Nb5 (FWHM =1.08 ± 0.10º). This fact can be related to several effects, for example, a smaller grain size or a higher value of microstrains for Nb10 than for Nb5 alloy. However, another effect can be considered after EDX results, where a wider distribution of particle composition was found for Nb10 than for Nb5 alloy. Therefore, the formed crystals are expected to present a wider distribution of lattice parameters. The shift of the position of the α-Fe (110) peak to lower values of 2θ is also bigger for Nb10 (2θ = 44.35 ± 0.05º) than for Nb5 alloy (2θ = 44.45 ± 0.05º). This result agrees with the higher amount of Nb in the Nb10 alloy, thus the crystals of the α-Fe phase must incorporate more Nb atoms in the lattice.

Respect to the amorphous halo formed for milling times larger than 200 h for Nb10 alloy, one explanation of this process is that Nb incorporation in the bcc Fe lattice destabilizes it, due to its very low solubility, allowing disordering and/or amorphous phase formation. Moreover, Nb content affects the velocity and energy necessary to form the amorphous phase [17]. For example, the $Fe_{82}Nb_6B_{12}$ alloy transforms to amorphous phase using a process control agent (PCA) and more energetic conditions [18], and the Fe_XNb_{X-1} system transforms to amorphous phase only for a composition range between X =0.3 to 0.7 [19].

In figure 10a, the lattice parameter of the α-Fe, *a*, is presented as a function of milling time. Before 20 h milling, the lattice parameter for both alloys (a= 2.864

±0.003 Å) is close to pure α-Fe (a =2.8665 Å) and, after 50 h, an increase is observed (due to the incorporation of Nb and B atoms in the bcc-Fe crystals). The value of a is higher for the alloy with more Nb content. However, the value obtained for Nb5 alloy is bigger than that found for $Fe_{85}Nb_6B_9$ supersaturated solid solution [20]. The lower Fe contamination observed in the present study could explain this difference.

From these results, it is possible to consider that the actual system after long milling times is formed by powder particles (in a certain compositional range) containing bcc-Fe(Nb,B) crystallites (which composition may depend on that of the powder particle). Taking into account the difficulty of separating the different effects contributing to the broadening of diffraction peaks (small crystal size, microstrains, existence of a lattice parameter distribution) the analysis has been simplified to calculate a minimum average grain size, $<D>$, (figure 10b) and a maximum value of microstrains, ε, (figure 10c), considering each individual effect as the only responsible for the broadening of the XRD peaks. $<D>$ reaches a minimum stable value after 50 h milling, being smaller for Nb10 alloy ($<D>$ =5 and 7 nm for Nb10 and Nb5, respectively). This result is comparable with those reported in other studies for similar alloys [1,20,[21]], as well as its dependency with the Fe content [20]. The maximum microstrains (just a limit value) reach ~2 % after 100 h milling for both alloys.

4.3.2 Mössbauer spectrometry

As milling times increases, the single site with HF =33 T is not enough to fit the spectra and new contributions are needed. The appearance of these new contributions, D1 and D2, is related to the presence of Nb and B in the neighborhood of Fe crystalline sites (in agreement with the increase of the lattice parameter from XRD results after t =50 h) and with Fe atoms outside crystals.

Intermetallics. Vol. 16. Núm. 9. 2008. Pag. 1073-1082
http://dx.doi.org/10.1016/j.intermet.2008.06.006

Figure 11 shows the fraction of Fe atoms in the different contributions. For Nb10 alloy, the disappearance of site-F after 100 h is observed, as well as the increase of the paramagnetic contributions (Nb rich environments) with the appearance of site-P after 200 h milling. However, no significant changes for Nb5 alloy are observed after 50 h milling. Therefore, microstructural changes are not expected in agreement with XRD results.

Mössbauer and XRD results allow us to distinguish two microstructures at the end of milling experiment performed (t = 400 h). On the one hand, for Nb5 alloy, there are α-Fe nanocrystals with pure bcc environments (site-F) and the presence of impurities taken into account by D2 contribution. This contribution also considers the interface effect. On the other hand, for Nb10 alloy, the pure bcc environment is no longer detected, and it is only possible to distinguish three Fe atomic environments: one ferromagnetic (possibly ascribed to residual crystallites) and two paramagnetic environments related with the amorphous phase formation observed by XRD. It is worth mentioning that all the powder particles of the Nb10 sample for 400 h milling moved in the vicinity of a small magnet, indicating that there are no pure paramagnetic powder particles but every particle must be composed of a mixture of ferromagnetic crystalline and paramagnetic amorphous phases.

4.4 Magnetic properties

In order to clarify the relationship between paramagnetic and ferromagnetic Fe sites at room temperature and the mixture of crystalline and amorphous phases composing the powder particles, the temperature dependence of magnetization, M(T), was measured from 77 to 440 K on Nb10 samples milled 100, 200, 300 and 400 h (figure 12). A Curie transition at T_C ~250 K is detected for milling times ≥200 h. This

transition can be ascribed to the amorphous phase detected by XRD, whereas the magnetization at higher temperatures corresponds to the α-Fe(Nb,B) nanocrystals. This Curie temperature is lower than that reported for amorphous alloys obtained by melt spinning with the same composition (325 K) [22]. Several aspects can explain this difference: the applied field used in the magnetization measurement (the higher the applied field the higher the measured value of T_C), the Cr contamination in the ball milling process (T_C decreases ~25 K/at. % Cr [23]), the Nb and B enrichment of the amorphous phase in our study, due to the presence of nanocrystals. The amount of amorphous phase can be estimated from both Mössbauer (low field contributions) and magnetization results. Both techniques agree showing an increase of the amount of amorphous phase with milling time. From Mössbauer results, the area fraction of the low field contributions increases from 49 to 77 % from 200 to 400 h milling. In the case of magnetic measurements, the magnetization fraction at 77 K ascribed to the amorphous phase increases from 32 to 69 % from 200 to 400 h milling. This fraction of magnetization should be related to the amount of amorphous phase in the samples. The differences between this magnetization fraction and the Fe atomic fraction in each phase obtained by Mössbauer spectroscopy can be explained by the different magnetic moments of the crystalline solid solution and the amorphous phase.

4.5 Thermal stability

Figure 13 shows the DSC scans of different as-milled samples taken at a heating rate of 40 K/min for both alloys. For short milling times, relaxation phenomena [20,24] start at ~700 K. However, for samples milled $t \geq 50$ h for Nb10 and $t \geq 20$ h for Nb5, a deviation from the baseline is detected at ~410 K. For Nb5 alloy milled 50 h or more, (after a supersaturated solid solution is formed), an exothermic peak is observed at ~900

K. For Nb10 alloy, after 400 h milling a clear exothermic peak is clearly observed at ~850 K.

In order to obtain activation energies, Q, by Kissinger method [25], scans at 5, 10, 20, 40 and 80 K/min were recorded on Nb5 and Nb10 samples milled 400 h, leading to an activation energy of 1.3 ± 0.1 eV for the broad exotherm at ~750 K of both alloys. For the DSC peaks detected for Nb5 alloy at 900 K and Nb10 at 850 K, Q =3.6 eV and 3.8 eV, respectively. Crystallization temperatures and activation energies of these exothermic processes are in agreement with values found in the literature for devitrification of amorphous/partially crystalline ribbons [6,22,26].

In order to clarify the nature of the different transformation peaks detected by DSC, XRD and Mössbauer techniques were applied to samples heated up to different temperatures (600, 800 and 1000 K). Figures 14 and 15 show XRD paterns of heated samples along with the corresponding as-milled ones for Nb5 and Nb10 alloys, respectively. Figures 16 and 17 show Mössbauer spectra and hyperfine field distributions of heated samples along with the corresponding as-milled ones for Nb5 and Nb10 alloys, respectively.

For Nb5 alloy heated up to 600 K, a slight decrease of the lattice parameter and a decrease of 17 % in FWHM of (110) α-Fe maximum is observed. After heating up to 800 and 1000 K, a continuous decrease in the lattice parameter down to that of pure α-Fe (see inset in figure 14) and in FWHM (22 and 28 %, respectively) is observed with respect to the as-milled sample. This can be ascribed to a progressive purification of the α-Fe phase and the decrease in the microstrain and crystal grain coarsening. However, it is worth mentioning that the FWHM of the sample heated up to 1000 K, 1.3 ±0.1º, yields a $\langle D \rangle$ ~7 nm. This indicated that the crystalline structure is stabilized by the Nb atoms rejected from the crystals, even after this temperature. Mössbauer technique

confirms these results, with a progressive increase of the 33 T contribution as heating temperature increases.

For Nb10 alloy, neither XRD nor Mössbauer show significant changes for the sample heated up to 600 K with respect to the as-milled one. Heating up to 800 K, yields a sharpening of the central region of the halo detected in the XRD pattern, as well as, an increase in the high field contributions (33 T sextet appears). This could be ascribed, analogously to Nb5 alloy, to the purification of the remaining α-Fe(Nb,B) phase, as the crystalline volume fraction does not change significantly (see inset figure 15). After heating up to 1000 K, crystallization of the amorphous phase occurs, evidenced by a clear (110) peak of the α-Fe phase. The lattice parameter of this phase is close to that of pure α-Fe (2.864 Å) and the average crystal size is ~9 nm. This indicated that the amorphous structure is almost still up to 800 K and the crystalline structure is achieved after the DSC peak detected at 850 K. These results are in agreement with Mössbauer spectra (see figure 17), where high field contributions increase.

Conclusions

From the present study on the mechanical alloying of the ternary FeNbB system, several conclusions can be remarked:

- The average powder particle size at long time milling is smaller for the alloy with the lowest Nb content.
- At long time milling, the composition of powder particles are not the same but a dispersion of ~10 % in their Fe content still exists.
- The Cr contamination linearly increases with the milling time for both alloys, being higher for the alloy with the highest Nb content.

- For milling times t ≥50 h, the only phase present in the samples is a bcc Fe(Nb,B) supersaturated solid solution for both alloys. After 400 h, only for the alloy with the highest Nb content, the presence of amorphous phase is evidenced by an amorphous halo observed by XRD, as well as the detection of an exothermic process in DSC ascribed to crystallization. This amorphous phase is stable up to ~850 K.
- For the alloy with the lowest Nb content, after 50 h milling no new Fe atomic sites appear, being the more important contribution at 33 T. However, for the alloy with the highest Nb content, the Fe atomic environment continuously evolves increasing the fraction of paramagnetic environments.
- The Curie transition of amorphous phase in the alloy with the highest Nb content is below room temperature (~250 K). This phase, detected by magnetization measurement for milling times t ≥200 h, was also detected by X-ray diffraction and Mössbauer spectroscopy techniques.

Acknowledgments

This work was supported by the Spanish Government and EU FEDER (Project MAT 2004-04618) and by the PAI of the Regional Government of Andalucía (Project P06-FQM-01823). J.J.I. acknowledges a fellowship from the Spanish Ministry of Education and Science. J.S.B. acknowledges a research contract from the Regional Government.

References

[1] C. Suryanarayana, Prog. Mater. Sci. 46 (2001) 1-184.

[2] H. Gleiter, Prog. Mater. Sci. 33 (1989) 223-315.

[3] H. Gleiter, Acta Mater. 48 (2000) 1-29.

[4] K. Suzuki, N. Kataoka, A. Inoue, A. Makino, T. Matsumoto, Mater. Trans. JIM 31 (1990) 743-746.

[5] A. Makino, T. Hatanai, A. Inoue and T. Matsumoto, Mater. Sci. Eng. A 226-228 (1997) 594-602.

[6] M.E. Mc. Henry, M.A. Willard, D.E. Laughlin, Prog. Mater. Sci. 44 (1999) 291-433.

[7] A. Hernando, M. Vázquez. T. Kulik, C. Prados, Phys. Rev. B 51 (1995) 3581.

[8] I. Chicinas, N. Jumate, Gh. Matei, J. Magn. Magn. Mater. 140-144 (1995) 1875-1876.

[9] S. Szabó, D.L. Beke, L. Harasztosi, L. Daróczi, Gy. Posgay, M. Kis-Varga, NanoStruc. Mater. 9 (1997) 527-530.

[10] Landolt-Börnstein, New Series, Vol. III/37A (Springer-Verlag, Berlin, 1997) 62-63, 173-174.

[11] R. A. Brand, J. Lauer, D. M. Herlach, J. Phys. F: Met. Phys. 13 (1983) 675-683.

[12] W. Lu, L. Yang, B. Yan, W. Huang, B. Lu, J. All. Comp. 413 (2006) 85-89.

[13] J.R. Stephens, W.R. Witzke, J. Less-Common Met. 48 (1976) 285-308.

[14] J.J. Ipus, J.S. Blázquez, V. Franco, A. Conde, Intermetallics 15 (2007) 1132-1138.

[15] J. M. Greneche, A. Slawska-Waniewska, J. Magn. Magn. Mater. 215-216 (2000) 264-267.

[16] B.Q. Zhang, L. Lu, M.O. Mai, Phys. B 325 (2003) 120-129.

[17] E. Jartych, D. Oleszak and J.K. Zurawicz, Hyp. Int. 136 (2001) 25-33.

[18] Z. Caamaño, G. Pérez, L.E. Zamora, S. Suriñach, J.S. Muñoz, M.D. Baró, J. Non-cryst. Solids. 287 (2001) 15-19.

[19] J.Y. Yang, T.J. Zhang, K. Cui, X.G. Li, J. Zhang, J. All. Comp. 242 (1996) 153-156.

[20] J.J. Suñol, A. González, J. Saurina, Ll. Escoda, P. Bruna, Mater. Sci. Eng. A 375-377 (2004) 874-880

[21] J.S. Blázquez, V. Franco, C.F. Conde, A. Conde, Intermetallics 15 (2007) 1351-1360.

[22] J. Torrens-Serra, J. Rodríguez-Viejo, M.T. Clavaguera-Mora, J. Non-Cryst. Sol. 353 (2007) 842-844.

[23] V. Franco, C.F. Conde, A. Conde, J. Magn. Magn. Mater. 303 (1999) 60-62.

[24] D. Oleszak, P.H. Shingu, J. Appl. Phys. 79 (1996) 2975-2980.

[25] D. Henderson, J. Non-cryst. Solids 30 (1979) 301-315.

[26] A. Makino, K. Suzuki, A. Inoue, T. Masumoto, Mater. Sci. Eng. A 179-180 (1994) 127-131.

Intermetallics. Vol. 16. Núm. 9. 2008. Pag. 1073-1082
http://dx.doi.org/10.1016/j.intermet.2008.06.006

Figure captions

Figure 1. SEM images of both alloys after selected milling times.

Figure 2. a) SE image, b) BSE image of a typical particle of Nb10 alloy after 2 h milling and c) EDX spectra of selected points indicated in a).

Figure 3. Experimental and simulated data of the average powder particles size as a function of the milling time for both alloys.

Figure 4. Histograms of the percentage of Fe content in total Fe+Nb content for both alloys at selected milling times.

Figure 5. Cr content as a function of milling time for both alloys. The slopes of the different fitted lines are also indicated.

Figure 6. XRD patterns of both alloys after selected milling times.

Figure 7. Mössbauer spectra and hyperfine magnetic field distributions for Nb10 alloy after selected milling times.

Figure 8. Mössbauer spectra and hyperfine magnetic field distributions for Nb5 alloy after selected milling times.

Figure 9. Experimental and simulated values of a) ΔC_{Fe} and b) C_{Fe} as a function of the milling time (experimental) and iteration steps (simulation). Horizontal lines at 88 and 94 at.% Fe correspond to the nominal values of Nb10 and Nb5, respectively. Iteration steps axes have been conveniently rescaled to show the agreement with the experimental data.

Figure 10. a) Lattice parameter, b) minimum crystal size and c) maximum microstrain as a function of milling time for both alloys.

Figure 11. Area fraction of the different Mössbauer contributions to the total fitting as a function of milling time for both alloys.

Intermetallics. Vol. 16. Núm. 9. 2008. Pag. 1073-1082
http://dx.doi.org/10.1016/j.intermet.2008.06.006

Figure 12. Magnetization curves as a function of temperature for Nb10 alloy after 100, 200, 300 and 400 h milling.

Figure 13. DSC scans at 40 K/min for both alloys after selected milling times. Symbols are superimposed over the curves to distinguish them.

Figure 14. XRD patterns for Nb5 alloy after different heated temperatures.

Figure 15. XRD patterns for Nb10 alloy after different heated temperatures.

Figure 16. Mössbauer spectra and hyperfine magnetic field distribution for Nb5 alloy after annealed treatment.

Figure 17. Mössbauer spectra and hyperfine magnetic field distribution for Nb10 alloy after annealed treatment.

Intermetallics. Vol. 16. Núm. 9. 2008. Pag. 1073-1082
http://dx.doi.org/10.1016/j.intermet.2008.06.006

Figure 1

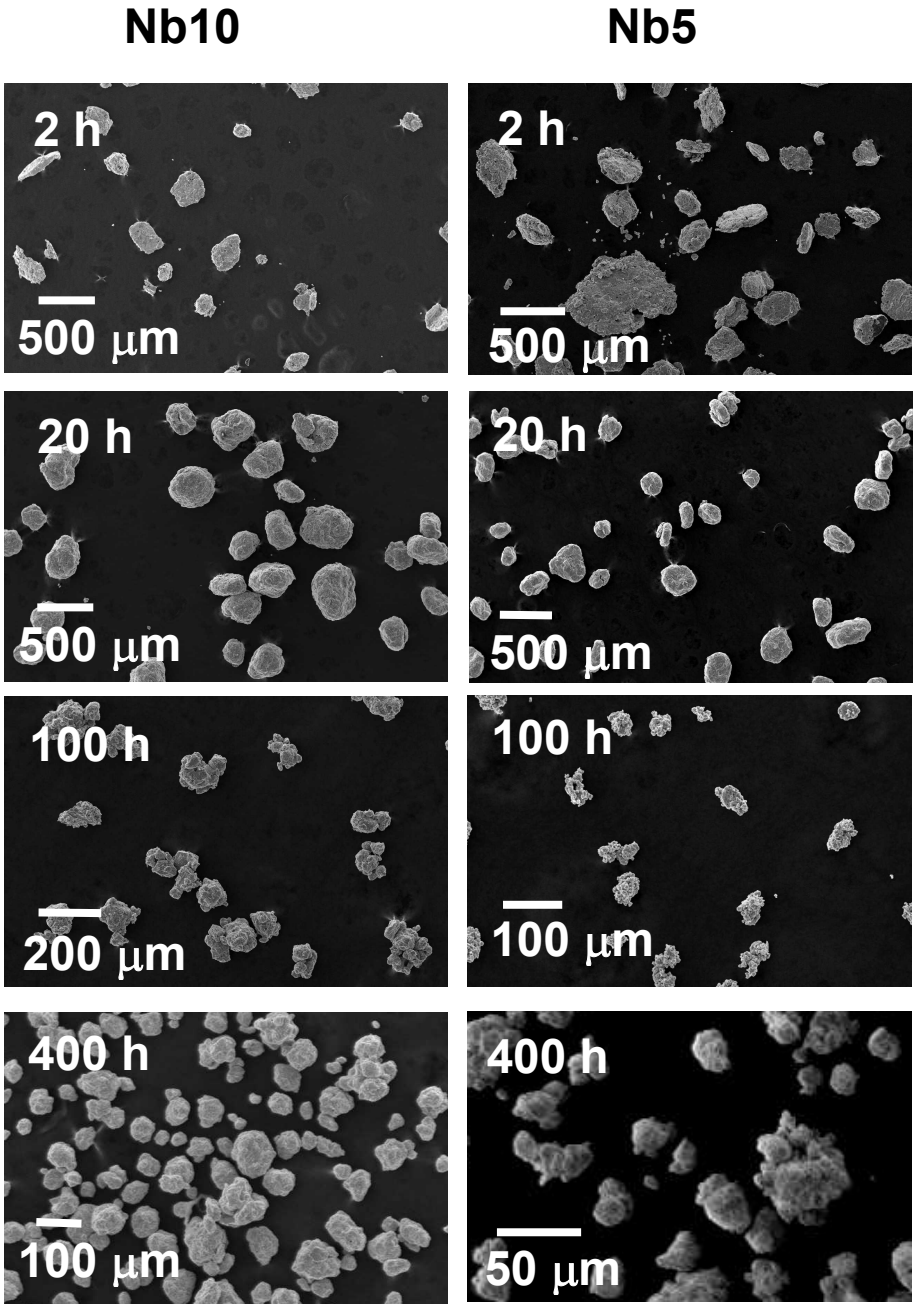

Intermetallics. Vol. 16. Núm. 9. 2008. Pag. 1073-1082
http://dx.doi.org/10.1016/j.intermet.2008.06.006

Figure 2

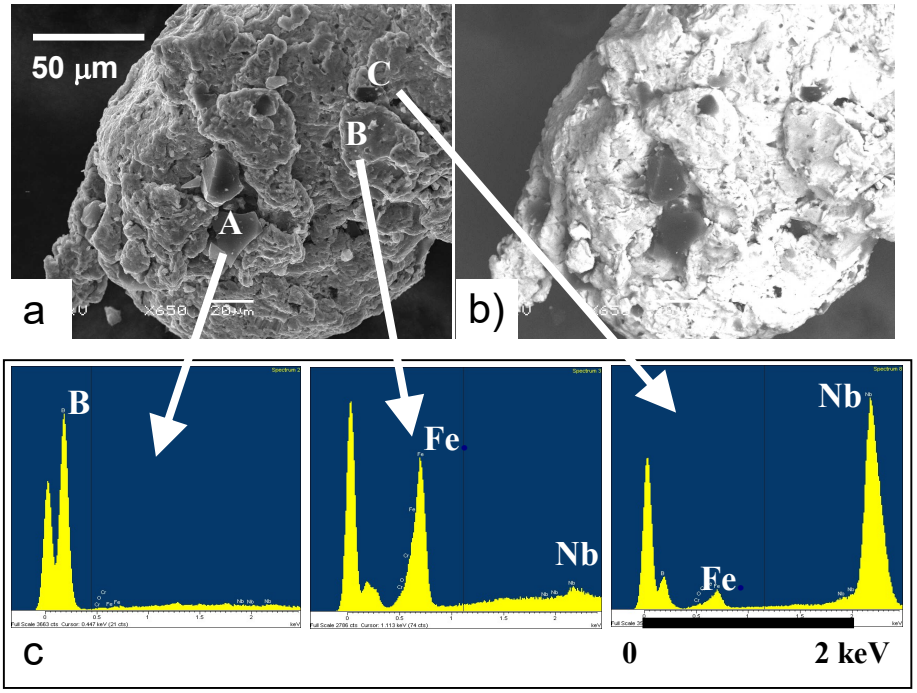

Intermetallics. Vol. 16. Núm. 9. 2008. Pag. 1073-1082
http://dx.doi.org/10.1016/j.intermet.2008.06.006

Figure 3

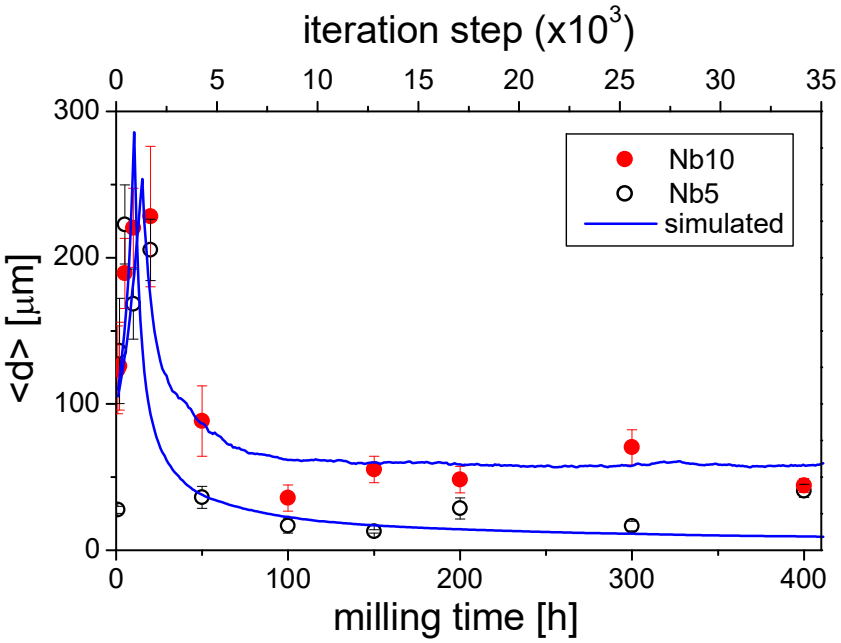

Intermetallics. Vol. 16. Núm. 9. 2008. Pag. 1073-1082
http://dx.doi.org/10.1016/j.intermet.2008.06.006

Figure 4

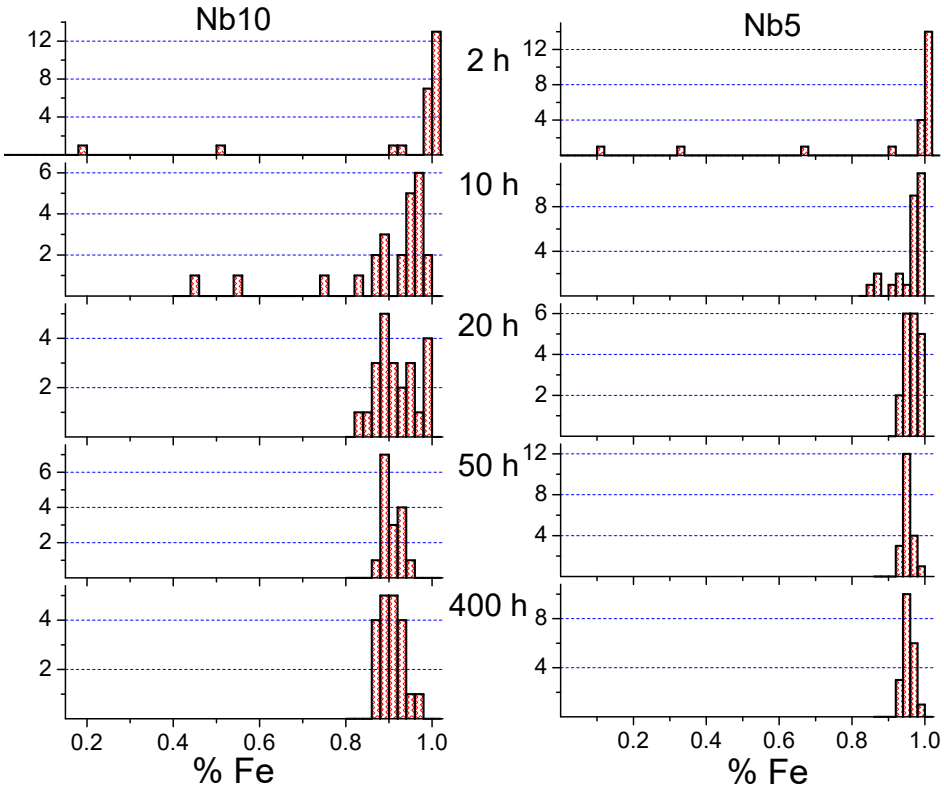

Intermetallics. Vol. 16. Núm. 9. 2008. Pag. 1073-1082
http://dx.doi.org/10.1016/j.intermet.2008.06.006

Figure 5

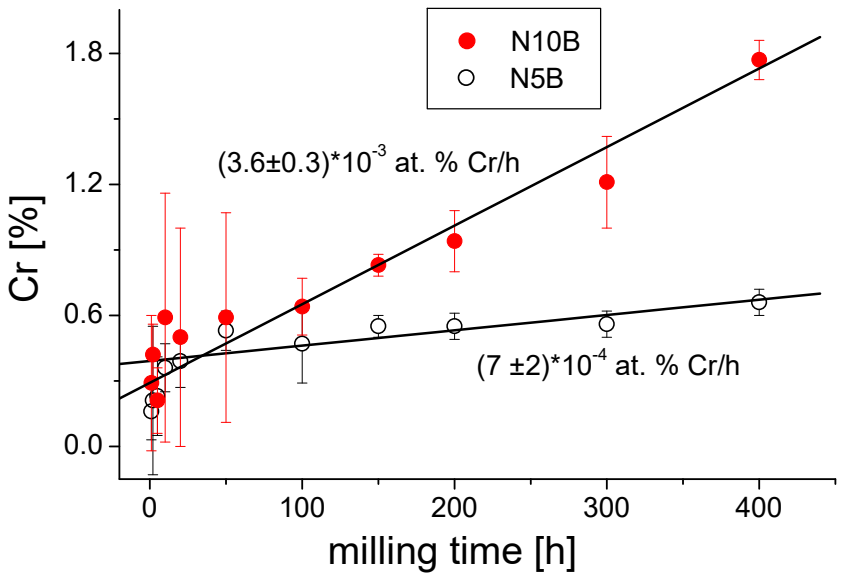

Intermetallics. Vol. 16. Núm. 9. 2008. Pag. 1073-1082
http://dx.doi.org/10.1016/j.intermet.2008.06.006

Figure 6

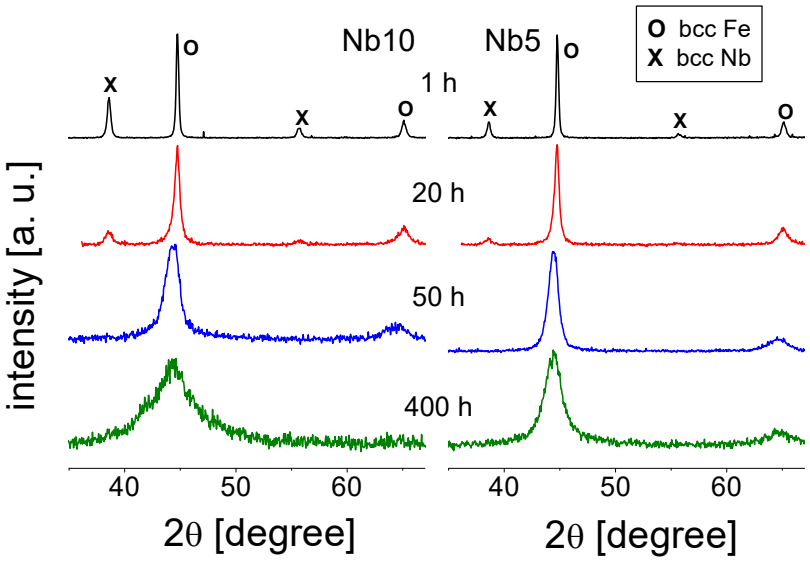

Intermetallics. Vol. 16. Núm. 9. 2008. Pag. 1073-1082
http://dx.doi.org/10.1016/j.intermet.2008.06.006

Figure 7

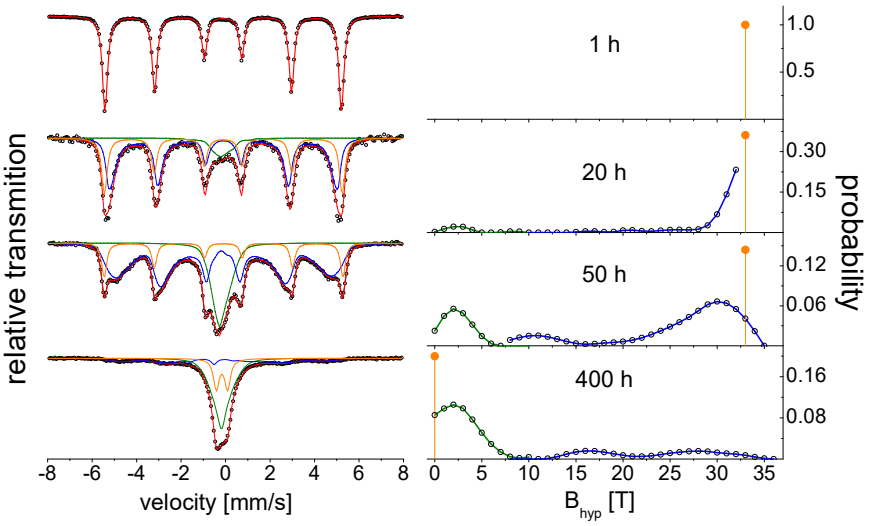

Intermetallics. Vol. 16. Núm. 9. 2008. Pag. 1073-1082
http://dx.doi.org/10.1016/j.intermet.2008.06.006

Figure 8

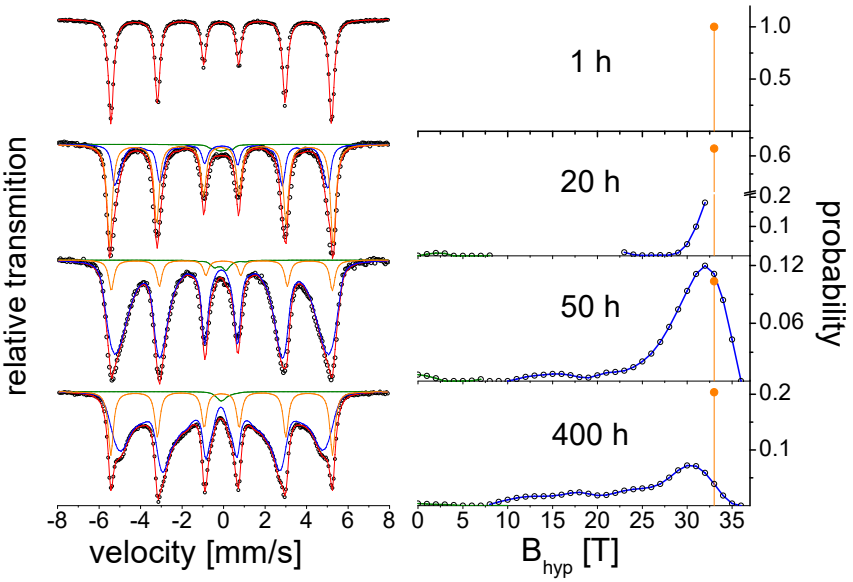

Intermetallics. Vol. 16. Núm. 9. 2008. Pag. 1073-1082
http://dx.doi.org/10.1016/j.intermet.2008.06.006

Figure 9

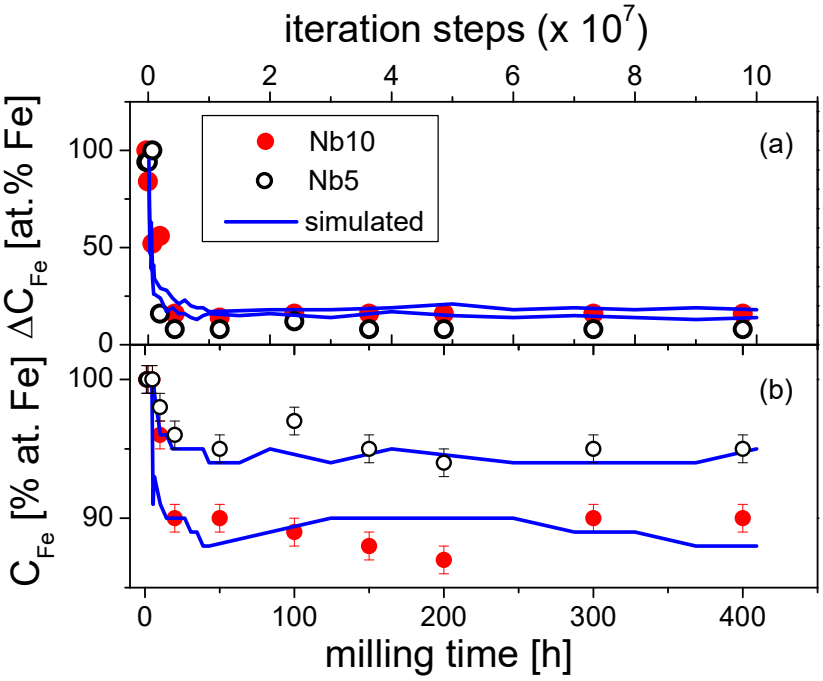

Intermetallics. Vol. 16. Núm. 9. 2008. Pag. 1073-1082
http://dx.doi.org/10.1016/j.intermet.2008.06.006

Figure 10

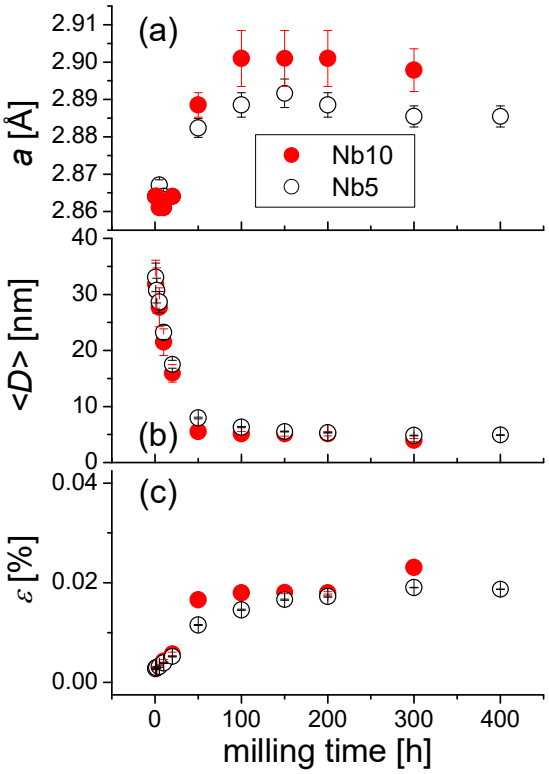

Intermetallics. Vol. 16. Núm. 9. 2008. Pag. 1073-1082
http://dx.doi.org/10.1016/j.intermet.2008.06.006

Figure 11

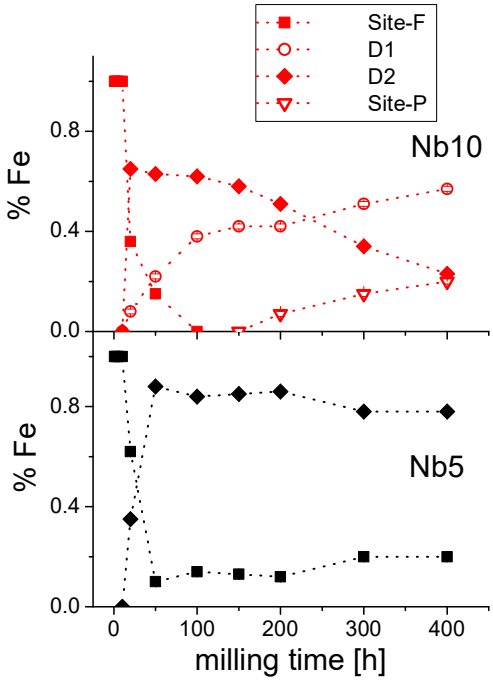

Intermetallics. Vol. 16. Núm. 9. 2008. Pag. 1073-1082
http://dx.doi.org/10.1016/j.intermet.2008.06.006

Figure 12

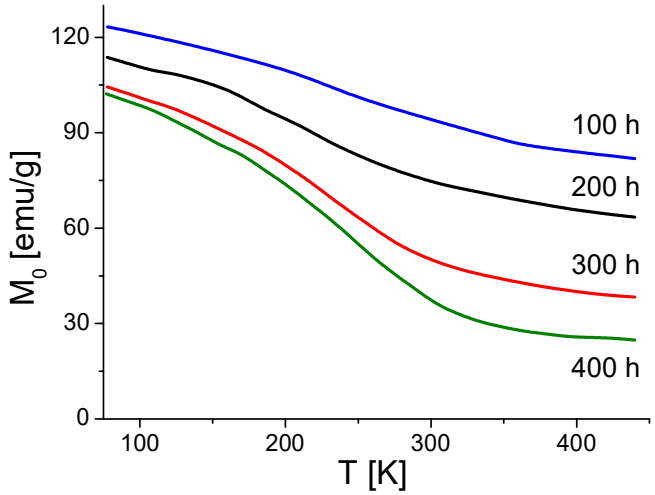

Intermetallics. Vol. 16. Núm. 9. 2008. Pag. 1073-1082
http://dx.doi.org/10.1016/j.intermet.2008.06.006

Figure 13

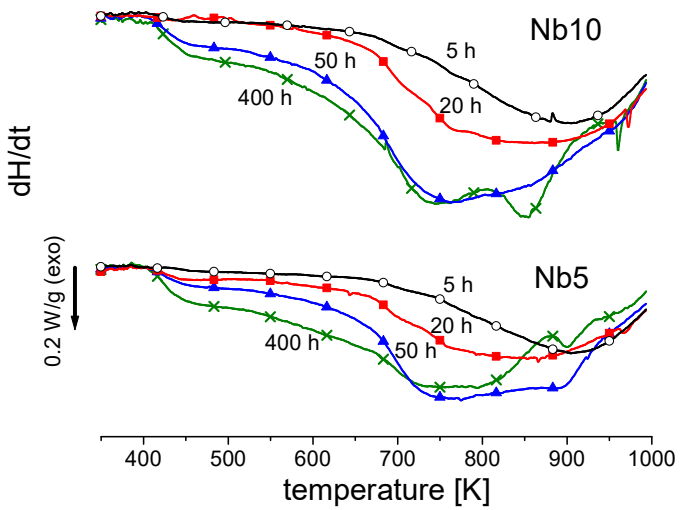

Intermetallics. Vol. 16. Núm. 9. 2008. Pag. 1073-1082
http://dx.doi.org/10.1016/j.intermet.2008.06.006

Figure 14

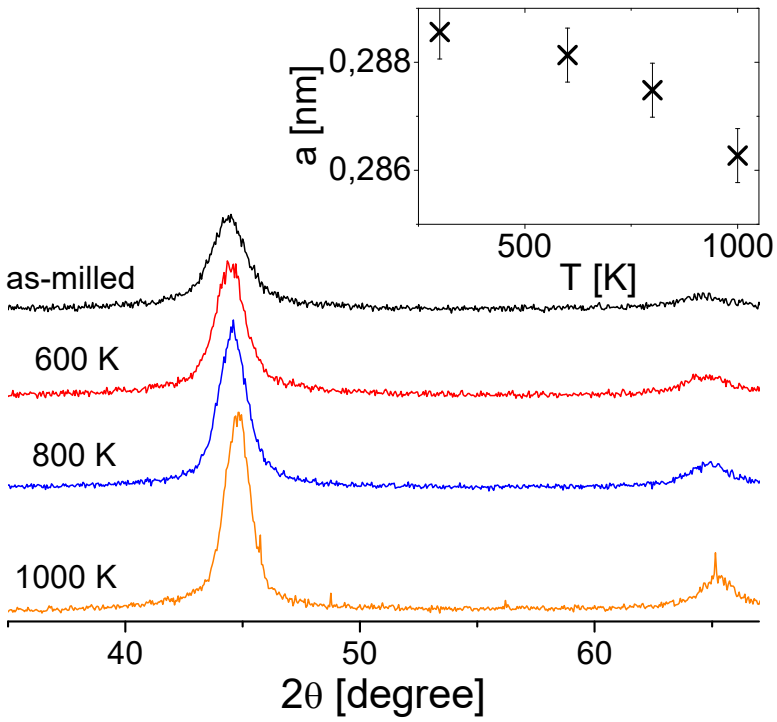

Intermetallics. Vol. 16. Núm. 9. 2008. Pag. 1073-1082
http://dx.doi.org/10.1016/j.intermet.2008.06.006

Figure 15

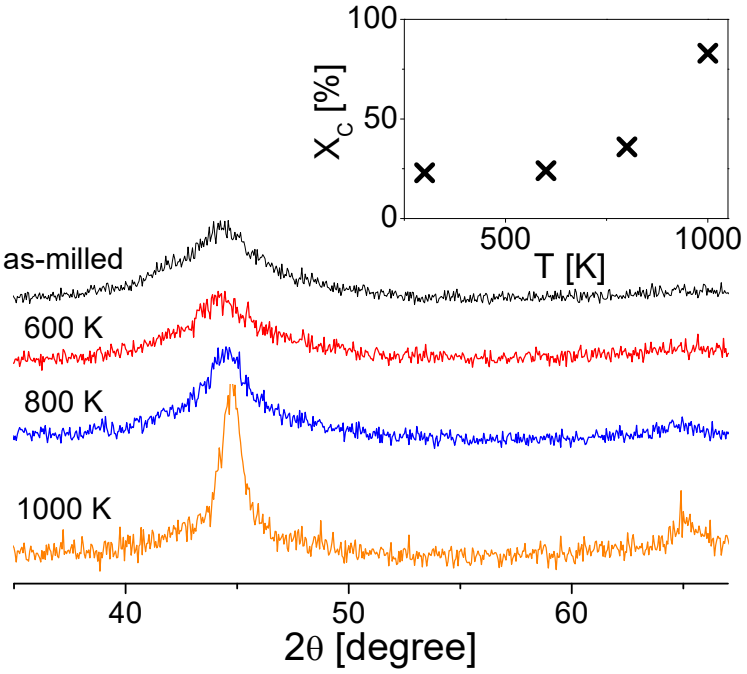

Intermetallics. Vol. 16. Núm. 9. 2008. Pag. 1073-1082
http://dx.doi.org/10.1016/j.intermet.2008.06.006

Figure 16

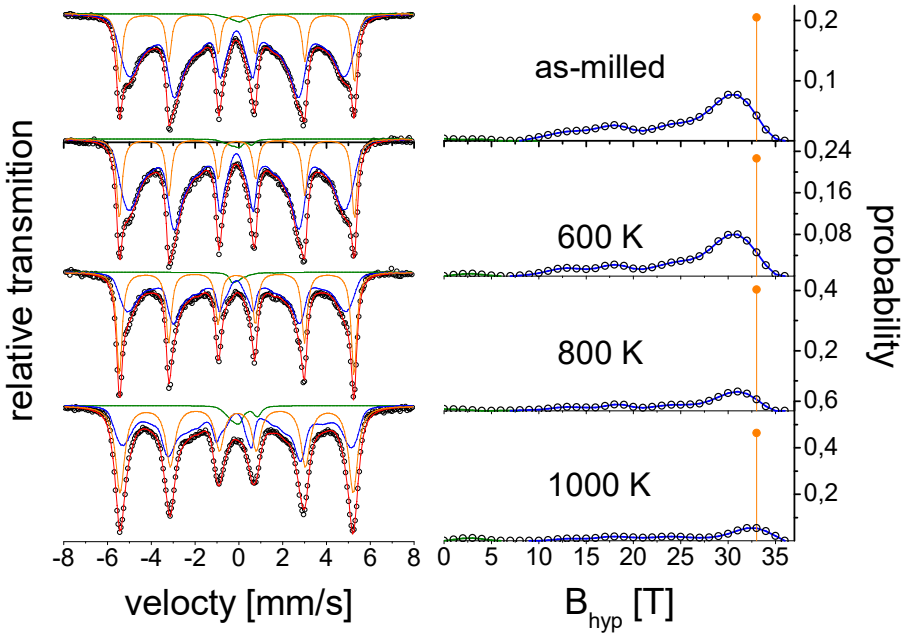

Intermetallics. Vol. 16. Núm. 9. 2008. Pag. 1073-1082
http://dx.doi.org/10.1016/j.intermet.2008.06.006

Figure 17